# Prediction challenge: First principles simulation of the ultrafast electron diffraction spectrum of cyclobutanone *⊗*

Special Collection: Prediction Challenge: Cyclobutanone Photochemistry

Jiří Suchan 🗓 ; Fangchun Liang 🗓 ; Andrew S. Durden 🗓 ; Benjamin G. Levine 🗷 🗓



J. Chem. Phys. 160, 134310 (2024) https://doi.org/10.1063/5.0198333





# Articles You May Be Interested In

Ultrafast photochemistry and electron diffraction for cyclobutanone in the  $S_2$  state: Surface hopping with time-dependent density functional theory

J. Chem. Phys. (July 2024)

The photochemistry of Rydberg-excited cyclobutanone: Photoinduced processes and ground state dynamics

J. Chem. Phys. (April 2024)

A CASSCF/MRCI trajectory surface hopping simulation of the photochemical dynamics and the gas phase ultrafast electron diffraction patterns of cyclobutanone

J. Chem. Phys. (March 2024)



**The Journal of Chemical Physics** 

Special Topics Open for Submissions

**Learn More** 



# Prediction challenge: First principles simulation of the ultrafast electron diffraction spectrum of cyclobutanone

Cite as: J. Chem. Phys. 160, 134310 (2024); doi: 10.1063/5.0198333 Submitted: 17 January 2024 • Accepted: 18 March 2024 •







Published Online: 4 April 2024

Jiří Suchan, De Fangchun Liang, De Andrew S. Durden, De and Benjamin G. Levine De Levi







# **AFFILIATIONS**

- <sup>1</sup> Institute of Advanced Computational Science, Stony Brook University, Stony Brook, New York 11794, USA
- Department of Chemistry, Stony Brook University, Stony Brook, New York 11794, USA

Note: This paper is part of the JCP Special Topic on Prediction Challenge: Cyclobutanone Photochemistry.

- <sup>a)</sup>Current address: Department of Chemistry, Wayne State University, Detroit, MI 48202, USA.
- b) Author to whom correspondence should be addressed: ben.levine@stonybrook.edu

#### **ABSTRACT**

Computer simulation has long been an essential partner of ultrafast experiments, allowing the assignment of microscopic mechanistic detail to low-dimensional spectroscopic data. However, the ability of theory to make a priori predictions of ultrafast experimental results is relatively untested. Herein, as a part of a community challenge, we attempt to predict the signal of an upcoming ultrafast photochemical experiment using state-of-the-art theory in the context of preexisting experimental data. Specifically, we employ ab initio Ehrenfest with collapse to a block mixed quantum-classical simulations to describe the real-time evolution of the electrons and nuclei of cyclobutanone following excitation to the 3s Rydberg state. The gas-phase ultrafast electron diffraction (GUED) signal is simulated for direct comparison to an upcoming experiment at the Stanford Linear Accelerator Laboratory. Following initial ring-opening, dissociation via two distinct channels is observed: the C3 dissociation channel, producing cyclopropane and CO, and the C2 channel, producing CH<sub>2</sub>CO and C<sub>2</sub>H<sub>4</sub>. Direct calculations of the GUED signal indicate how the ring-opened intermediate, the C2 products, and the C3 products can be discriminated in the GUED signal. We also report an a priori analysis of anticipated errors in our predictions: without knowledge of the experimental result, which features of the spectrum do we feel confident we have predicted correctly, and which might we have wrong?

Published under an exclusive license by AIP Publishing. https://doi.org/10.1063/5.0198333

#### I. INTRODUCTION

Ultrafast spectroscopic measurements<sup>1</sup> ushered in a new era of chemistry, in which the microscopic motions of molecules could be observed directly. However, while one might dream of a "molecular movie," in which the states of individual electrons and nuclei are recorded as a function of time in intricate detail, realistic ultrafast measurements necessarily involve the projection of molecular dynamics into a reduced-dimensional representation via a limited set of observables. As such, from very early on, the simulation of ultrafast dynamics has been an invaluable partner of experiment.<sup>2-6</sup> Where experiment provides a lossy projection of real chemical dynamics, simulated dynamics may be analyzed in their full dimensionality. However, simulated dynamics are necessarily approximate in all but the smallest systems. Despite three decades of intense effort, the inherent complexity of modeling many-body quantum dynamics drives an ongoing effort to develop practical approximations, <sup>7–12</sup> benchmark them for accuracy, 13-15 and develop high-performance, user-friendly software implementations. 16-20 Simulation has been very successfully applied as a tool for *a posteriori* analysis, connecting experimental signatures to actual molecular motions that cannot be unambiguously inferred from low-dimensional experimental data.<sup>21-31</sup>

Dynamics simulations alone are valuable, but the direct computation of ultrafast experimental observables from molecular dynamics simulations enables a much more definitive assignment of spectroscopic features. 32-45 Without direct simulation of the experimental observable, the connection between theory and experiment is often made by comparing lifetimes. Because lifetimes often depend exponentially on computed energies, which may themselves carry significant errors, lifetimes are among the most error-prone quantities one can compute. Most other observables do not suffer from an exponential amplification of errors in the potential energy surface (PES); therefore, explicit simulation of experimental observables (e.g., time-resolved spectra or scattering signals) enables a more direct connection between theory and experiment. Armed with computed observables, one may make definitive assignments even when simulated lifetimes have significant errors.

As light sources continue to advance,  $^{46,47}$  novel theoretical methods are required to connect to the new experiments they enable.  $^{48-53}$  Gas phase ultrafast electron diffraction (GUED) experiments  $^{54-60}$  offer a particularly appealing target for direct simulation, given the intuitiveness of the observable (interatomic distances). Because even very low levels of electronic structure theory can predict bond lengths with errors of only a few percent, the simulation of GUED enables an extraordinarily tight connection between experiment and theory.  $^{60-64}$ 

With dynamical simulation now established as an essential partner to experiment in ultrafast science, it is natural to ask a more ambitious question: to what extent can simulation predict ultrafast dynamics a priori? With this question in mind, the community conceived a prediction challenge to which this article responds. Over the past 15 weeks, we have attempted to predict the signal of an upcoming GUED experiment on cyclobutanone to be carried out at the Stanford Linear Accelerator Laboratory<sup>65</sup> (SLAC) in the days following the submission of this work.<sup>66</sup> Herein, we report the resulting prediction. We also report a brief analysis of the predicted dynamics and how they will manifest in the experimental signal. Finally, with the goal of testing our own understanding of our methods, we present predictions of what errors we might anticipate in our computed experimental signal. By taking part in this collective effort, we hope to better understand the limits of ultrafast theory and identify directions for the development of practical tools capable of definitively predicting ultrafast dynamics.

#### II. METHODS

#### A. Nonadiabatic dynamics

We will simulate the nonadiabatic dynamics of cyclobutanone using a novel *ab initio* implementation of the Ehrenfest with collapse to a block (TAB) method, which is described in detail in Refs. 67 and 68. Here, we provide a brief introduction to the basic features of the method. We ran our simulations in an open source software package, TAB-DMS.<sup>69</sup>

The TAB mixed quantum-classical method was developed to correct errors associated with the mean-field nature of Ehrenfest dynamics<sup>70</sup> via a decoherence correction that provides an accurate and efficient treatment of systems with many electronic states. Nuclei are propagated classically, with the force vector,  $F_{\rm MF}$ , calculated in a mean-field fashion,

$$F_{\rm MF}(t) = -\frac{\mathrm{d}}{\mathrm{d}R} \frac{\langle \Psi(t) | H(t) | \Psi(t) \rangle}{\langle \Psi(t) | \Psi(t) \rangle},\tag{1}$$

averaging the effect of electronic Hamiltonian, H(R(t)), on the time-dependent electronic wave function  $\Psi(t)$ . Using the Verlet algorithm, we propagate the nuclear positions, R, in discrete time steps.

The TAB decoherence correction is based on an assumption of exponential decay of electronic coherences at a rate given by the difference between gradients of each pair of potential energy surfaces (PESs). 71.72 At the end of each nuclear time step,  $\Delta t$ , the loss of coherence is incorporated into an approximate electronic density matrix,  $\rho^d$ , which represents the mixed electronic state that arises from decoherence during a single time step. This matrix is generated from the coherent mean-field electronic density matrix,  $\rho^c$ , associated with a given trajectory. The populations are taken directly from the coherently propagated mean-field density matrix,

$$\rho_{ii}^d = \rho_{ii}^c(t + \Delta t),\tag{2}$$

while the off-diagonal elements are scaled according to

$$\rho_{ij}^d = \rho_{ij}^c(t + \Delta t)e^{\frac{-\Delta t}{\tau_{\text{eff},ij}}}.$$
 (3)

The pivotal quantity here is the effective state-pairwise decoherence time,  $\tau_{\text{eff},ij}$ . Our approach starts from the widely used estimate of the decoherence time derived by Bittner and Rossky,  $7^{1,72}$ 

$$\tau_{ij}^{-2} = \sum_{n} \frac{\left(F_{i,\eta}^{\text{avg}} - F_{j,\eta}^{\text{avg}}\right)^{2}}{\hbar^{2} \alpha_{\eta}}.$$
 (4)

The sum runs over all degrees of freedom, indexed  $\eta$ , adding the differences of electronic-state-specific forces,  $F_i^{\text{avg}}$ , averaged over the beginning and the end of a time step. Parameter  $\alpha_n$  represents the atom-specific width of the Gaussian wavepacket and can, therefore, be determined without empirical fitting by fitting the harmonic ground state vibrational wave function.<sup>73</sup> In doing this fitting, we constrain the widths such that each degree of freedom associated with a particular atom type (C, H, or O) has the same width as all others of the same type. The reduced Planck constant is  $\hbar$ . The decoherence time represents the decay of the overlap between Gaussian wave packets on a pair of linear, non-parallel PESs. This overlap is a Gaussian function of time, and the decoherence time corresponds to its width. The effective decoherence time,  $\tau_{\text{eff},ij}$ , is computed from the Bittner–Rossky decoherence time,  $\tau_{ij}$ , by integrating over an approximate history of the dynamics, as detailed in Ref. 68. In so doing, we are able to effectively treat the coherence decay as Gaussian rather than exponential.

Next, we use a stochastic procedure (described in detail in Ref. 74) to collapse the electronic wave function to a new pure linear combination of a subset of occupied adiabatic states. This procedure is designed such that the ensemble average of the resulting electronic density matrix (averaged over all possible outcomes) is  $\rho^d$ . The velocity is rescaled at every time step where collapse occurs for conservation of the total energy. Although we have recently developed an approximate scheme for extending TAB to very large numbers of electronic states, 74 it is not necessary here.

In order to compute the GUED spectrum, a set of 150 trajectories was initiated on the  $S_2$  (3s Rydberg) electronic state. Initial nuclear positions and momenta were sampled from the Wigner distribution function computed in the harmonic approximation. The

ground state minimum geometry and frequencies were computed via B3LYP with a  $6-311++G^{**}$  basis. No attempt was made to account more specifically for the excitation wavelength via the initial conditions. All observables are taken as averages over this ensemble.

# **B. Electronic structure**

# 1. Propagation algorithm

To propagate the electronic structure, we use our highperformance implementation of the time-dependent complete active space configuration interaction method (TD-CASCI). The electronic wave function,  $\Psi(t)$ , is represented as a linear combination of Slater determinants,  $\Phi_I$ , with time-dependent expansion coefficients  $C_I(t)$ ,

$$\Psi(t) = \sum_{I} C_{I}(t)\Phi_{I}. \tag{5}$$

Their propagation is handled by numerically solving the time-dependent Schrödinger equation,

$$i\dot{\mathbf{C}}(t) = \mathbf{H}(t)\mathbf{C}(t),\tag{6}$$

via symplectic split operator integration.77

The TAB dynamics driver is interfaced with the TD-CASCI propagation scheme, providing a robust and efficient method to simulate nonadiabatic dynamics. The TD-CASCI algorithm is implemented in a development version of the TeraChem electronic structure package. 75,76,78–83 The combination of graphics processing unit (GPU)-acceleration and direct implementation of *HC* products allows efficient propagation in the full space of states without the need to build any data structures with the full dimension of the electronic Hamiltonian.

In theory, this combination allows us to model any incoming pulse directly in the dynamics while capturing possible initial coherences. Due to the time constraints of the project, all of our dynamics start directly in a given state. This is further justified by the known form of the experimental pulse, which intends to excite the first 3s Rydberg state. To ensure energy conservation, the electronic time step was set to 2 and the nuclear time step to 0.12 fs. The simulations aim to capture 500 fs of the post-excitation process.

# 2. Electronic ansatz selection

Cyclobutanone photochemistry has been examined in several past quantum chemical studies. 84-86 Several important points on the PES have been identified: So and S1 minima and a transition state, which seems to govern the overall pre-dissociative dynamics on S<sub>1</sub>. A visualization of the main reaction pathways is depicted in Fig. 2. Our simulations predict that most of the S<sub>2</sub> population transition to the S<sub>1</sub> state via a closed-ring conical intersection. In S<sub>1</sub>, the molecule must overcome a ring-opening barrier before dissociating via two main reaction channels labeled as C2 for CH2CO + C2H4 products and C3 for C<sub>3</sub>H<sub>6</sub> (cyclopropane) + CO products. Based on past publications, it appears that multi-state second-order perturbation theory (MS-CASPT2) on the complete active space self-consistent field (CASSCF) wave function accurately captures the significant correlation effects. Quite large active spaces, ranging from 6 electrons in 6 orbitals (6,6) up to 12 electrons in 11 orbitals (12,11), were used to capture the bond-breaking reaction channels. These studies

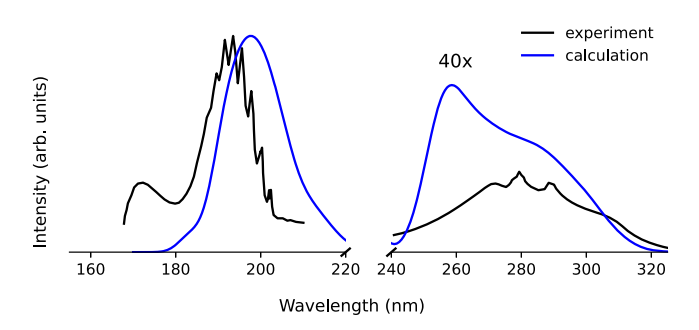


FIG. 1. Normalized experimental<sup>88,89</sup> and calculated absorption spectrum using the selected FOMO-CASCI(8,11)/6-311+G\* method.

usually state-averaged only over two valence singlet electronic states; thus, less is known about the 3s Rydberg state.

Regarding the role of triplet states, intersystem crossing from the  $S_1$  state seems to take place on nanosecond timescales. Ref. It dominates only near the onset of the absorption spectrum, where there is not enough energy to traverse the  $S_1$  barrier and relax via internal conversion (IC). Therefore, we will not consider ISC in our simulations.

The upcoming experiment will excite to the 3s Rydberg state (S<sub>2</sub>) with 200 nm (6.2 eV) laser light, which is well above the darker  $n \to \pi^*$  (S<sub>1</sub>) state (280 nm; 4.4 eV). The experimental absorption spectrum <sup>88,89</sup> (Fig. 1) reveals that the selected wavelength corresponds to the onset of the 3s Rydberg state. We further observe the 3p Rydberg states in the range of 170–180 nm (6.9–7.3 eV). Since states seem well separated, we need to choose an electronic structure ansatz that will reliably describe the overall S<sub>2</sub>  $\to$  S<sub>1</sub>  $\to$  S<sub>0</sub> internal conversion process but need not describe the 3p Rydberg states and above.

We tested several combinations of multireference methods and active spaces, as the choice of orbitals can play an important role in determining the accuracy of CASCI-based dynamics simulations. 90 Since the most important task is to capture the predissociation phase accurately, we aimed for the best agreement of relative state energies in several structures. To this end, we choose a floating occupation molecular orbital complete active space configuration interaction method (FOMO-CASCI) ansatz. 91,92 We choose an active space of 8 electrons in 11 orbitals (8,11), including the ground state-occupied non-bonding orbitals of the O atom and the  $\pi$  and  $\sigma$  bonding orbitals on the carbonyl group. The ground statevirtual orbitals in the active space include the carbonyl  $\pi^*$  orbital and two  $\sigma^*$  orbitals, as well as the 3s,  $3p_x$ ,  $3p_y$ , and  $3p_z$  Rydberg orbitals. This selection is capable of describing the relevant Rydberg and valence states, as well as the bond dissociation processes to expected products. The FOMO-CASCI method uses a fictitious electronic temperature, which we set to 0.3 Ha. The employed 6-311+G\* basis set includes diffuse functions that are necessary for the description of Rydberg states.

To establish the quality of the selected FOMO-CASCI method, we make a comparison to the experiment. Represent the calculated absorption spectrum, which is computed by compounding vertical spectra computed at a set of Wigner-sampled geometries with 0.1 eV Gaussian line broadening. The excitation energies at

TABLE I. FOMO-CASCI vertical excitation energies calculated with the (8,11) active space and 6-311+G\* basis at the B3LYP-optimized S<sub>0</sub> minimum geometry. Experimental data based on spectral maxima.

State	Character	FOMO-CASCI	Experiment <sup>88,89</sup>
$\overline{S_1}$	$n \rightarrow \pi^*$	4.65	4.4
$S_2$	$n \rightarrow 3s$	6.32	6.2

the ground state minimum geometry are presented in Table I, with experimental absorption maxima for comparison. In both cases, we observe that the FOMO-CASCI gap between valence and Rydberg states is slightly smaller than observed experimentally, but overall, the FOMO-CASCI method is very accurate in the Franck-Condon region.

# C. Calculation of GUED signal

To simulate the GUED signal, we calculate time-dependent 1D electron diffraction patterns. They can also be converted to pair distribution functions (PDFs). Both representations are directly comparable to the experiment.

To calculate the GUED signal, we utilize the independent atom model (IAM), closely following the procedure described by Centurion et al.<sup>54</sup> First, we calculate the electron scattering amplitudes from the individual atoms. These atomic form factors (AFFs), f(s), were calculated using the ELSEPA program<sup>93</sup> using parameters for the SLAC facility. The scattering intensity of a molecule, I(s), as a function of momentum transfer, s, is composed of individual  $(I_{at})$  and pairwise  $(I_{mol})$  contributions of scattering amplitudes. For a gas phase sample, we assume the following simplified

$$I(s) = I_{\text{at}} + I_{\text{mol}} = \sum_{i=1}^{N} |f_i(s)|^2 + \sum_{i=1}^{N} \sum_{j=1, j \neq i}^{N} f_i^*(s) f_j(s) \frac{\sin(sr_{ij})}{sr_{ij}}.$$
 (7)

Here, the i, j indices loop over N atoms. Interatomic distances are denoted as  $r_{ii}$ . Due to the nominal  $s^{-5}$  dependence of the molecular scattering intensity, we work with a more suitable form, the modified scattering intensity,

$$sM(s) = s\frac{I_{\text{mol}}}{I_{\text{ot}}}. (8)$$

Finally, the real-space PDF, P(r), which describes the probability of atom pairs being at a given distance, can be obtained by the sine transformation.

$$P(r) = r \int_0^\infty sM(s) \sin(sr) ds. \tag{9}$$

To consider experimental limitations, we should integrate this equation between the limits of the detector,  $s_{\min}$  and  $s_{\max}$ , and add a damping factor that avoids artifacts of the transformation,

$$P(r) = r \int_{s}^{s_{\text{max}}} sM(s) \sin(sr) e^{-\alpha s^2} ds.$$
 (10)

The experimental resolution for the upcoming measurement is 1-10 Å<sup>-1</sup>. Nevertheless, the data between 0 and  $s_{min}$  are usually interpolated to avoid artifacts in the PDF. Therefore, in our calculations, we used the full 0-10 Å<sup>-1</sup> range to emulate the instrumental limitations, and we employed a damping factor  $\alpha$ of 0.04 Å<sup>2</sup>. PDFs computed at specific important geometries are depicted in Fig. 2. In dynamics simulations, the modified scattering intensity is calculated as an average over the ensemble of trajectories at a given time. We also calculate the difference pair distribution function ( $\Delta$ PDF) by subtracting the scattering signal at time zero [in Eq. (8)] to better observe various relaxation channels. We report two different representations of the experimental signal: the signal computed with the temporal resolution of the simulation (assuming the pump pulse instantaneously excites the molecule to S<sub>2</sub>), and a second version convoluted with an 80 fs FWHM temporal Gaussian, matching the anticipated experimental cross-correlation.

#### III. RESULTS

#### A. TAB simulations

The average adiabatic electronic populations predicted by our TAB simulations are displayed in Fig. 3. The lines represent the mean values over the ensemble of trajectories, and the shaded areas show the 95% confidence interval based on the binomial distribution. (This confidence interval reflects only the error associated with trajectory sampling, not errors related to physical approximations.) Following excitation, the molecule undergoes rapid relaxation through a conical intersection (CI) to reach the S1 state. Half of the original population transitions during the first 12 fs. However, it takes 65 fs until the S2 population decays below 0.1. Analysis of the minimum energy conical intersection between S2 and S1 (Fig. S1) indicates that it is strongly symmetry broken, with one of the two symmetry-equivalent CO-CH<sub>2</sub> bonds stretched to 1.83 Å. This indicates that there is an initial impulse toward ring opening on S<sub>2</sub>. Once on S<sub>1</sub>, the molecule relaxes to the ground state via the respective CI. This requires crossing of a ring-opening transition state, which may prolong the relaxation time. After reaching the ground state, we observe the usual relaxation channels for C2 and C3 products.

In addition to these main pathways, 19% of the population is observed to undergo ring-opening directly in the S2 state, which contributes to the prolonged S2 relaxation. The molecule then transitions to either S<sub>1</sub> or S<sub>0</sub> at various points in time. Both C2 and C3 channels are observed following relaxation to S<sub>0</sub>. Within our sampling of 150 trajectories, it is not obvious that ring-opening on S<sub>2</sub> impacts the photoproduct distribution.

In total, most trajectories form the C3 products (60%), although the cyclization to cyclopropane is not always completed within our 500 fs simulation window. C2 products are created in 28% of cases. In the remaining 12%, we observe some larger fragmentation of the original molecule, including CO formation and hydrogen dissociation. The presented product analysis does not include trajectories that terminated prematurely or did not lead to the complete ring-opening reaction. Ultimately, 70 and 32 trajectories followed the C3/C2 channels, respectively, yielding a branching

We note that our trajectories were facing convergence issues. Only 32% of them reached the 500 fs mark (see Fig. S2 for details). Cyclobutanone photodissociation seems to present a challenge for electronic structure methods, mainly due to the formation of various

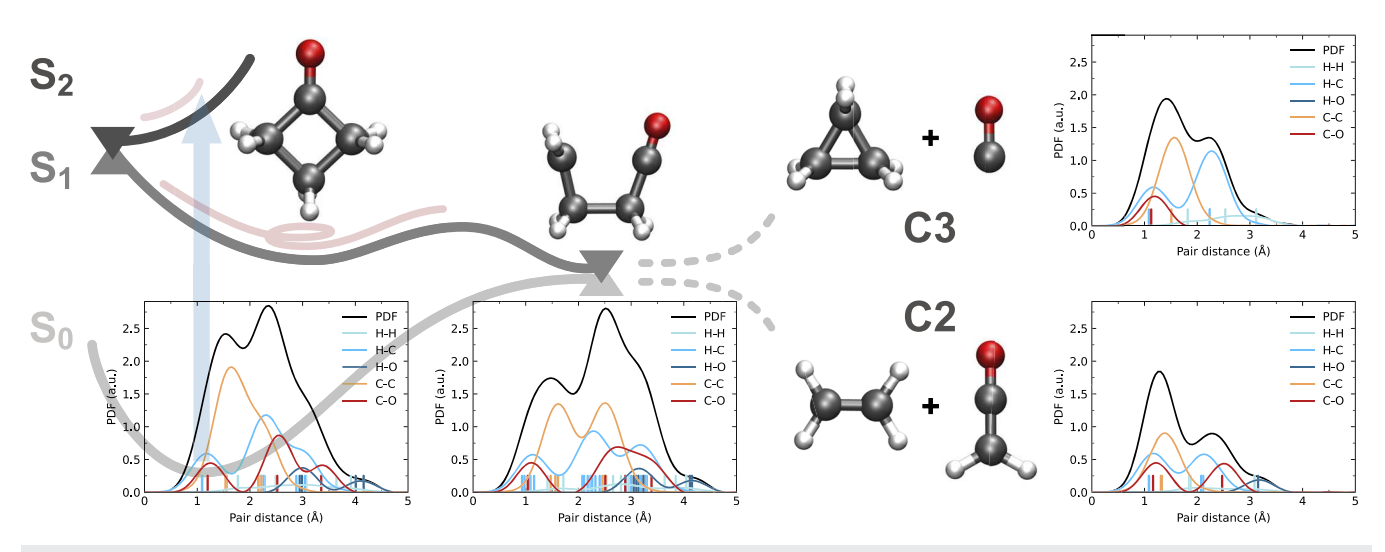
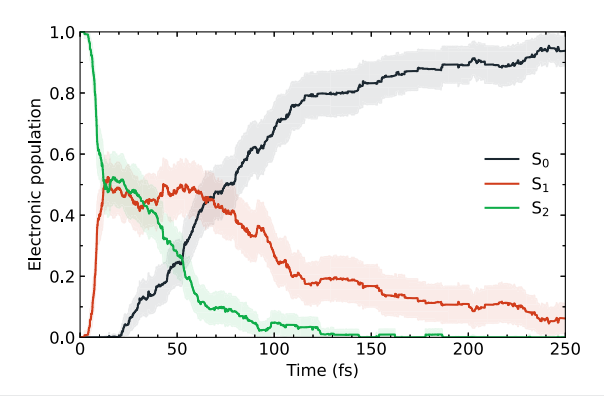


FIG. 2. Visualization of the main photochemical pathways of cyclobutanone following excitation to S<sub>2</sub>. The expected PDF signal calculated using the IAM model for the initial molecule, open ring structure, and products (C2 and C3) with individual contributions from atomic pairs.



molecular species in the process. This additional source of uncertainty in our prediction is the direct result of the artificial time constraints of the prediction challenge.

From the TAB dynamics, we simulate the time-dependent  $\Delta$ PDF signal. Figure 4 displays the resulting signal at simulation resolution [panel (a)] and convoluted by the experimental cross-correlation [panel (b)]. There is a faint signal in the first tents of fs when the initial  $S_2 \rightarrow S_1$  relaxation takes place. After that, we start to observe a new signal above the previously blank 3 Å threshold. This is due to the ring-opening process and subsequent dissociation into distinct molecular products. Since the  $\Delta$ PDF fingerprints of individual intermediates and products are rather similar, it is difficult to discern between them using this plot. For easier analysis, we present time slices of the  $\Delta$ PDF data in Fig. 4(d). The corresponding plot in momentum space—the difference modified scattering intensity ( $\Delta$ sM)—is shown in Fig. 4(c). Reference signals associ-

ated with three static geometries are presented for comparison: a representative open ring intermediate structure and the C2 and C3 products. We have chosen the FOMO-CASCI-optimized  $S_1\text{-}S_0$  minimal energy conical intersection structure (pictured in Fig. 2) to represent the ring-opened region of the PES. We do not mean to imply that the signal in this region necessarily corresponds to the detection of population at the conical intersection. However, it carries the ring-opening character that is specific to product formation. The rest of the reference structures were optimized at the  $B3LYP/6\text{-}311\text{+}G^{\ast}$  level.

At 50 fs, both the  $\Delta PDF$  and difference in modified scattering intensity ( $\Delta sM$ ) exhibit features that are characteristic of the representative ring-opened ( $S_1$ – $S_0$  conical intersection) structure. In momentum space, the first negative peak (between 0 and 2 Å<sup>-1</sup>) closely mirrors that of the ring-opened structure, and there is a pronounced negative peak near 6 Å<sup>-1</sup> that does not appear in either the C2 or C3 products. In the  $\Delta PDF$ , there is a large positive peak just below 4 Å that is characteristic of the ring-opened structure.

At later times, the signals evolve in a way that reflects the dissociation. In momentum space, the first negative peak intensifies and shifts to lower momentum (now below 1  ${\rm \AA}^{-1}$ ) upon dissociation. In position space, the large peak near 4  ${\rm \AA}$  loses intensity as the ring-opened structure dissociates. In addition, the broad negative feature between 1 and 3  ${\rm \AA}$  intensifies.

A detailed analysis of this broad negative feature allows discrimination between the C2 and C3 products. The lower-distance portion of this feature ( $\sim$ 1.5 Å) corresponds to the loss of carbon–carbon bonds. The reactants contain four C–C bonds. The C3 products have three C–C bonds (all in cyclopropane), while the C2 product has only two (one in each product). Thus, as the ring-opened structure disappears, a more pronounced shoulder at  $\sim$ 1.5 Å is indicative of a lower C3/C2 branching ratio. Differences are also observed in the momentum-space representation. Between 4 and

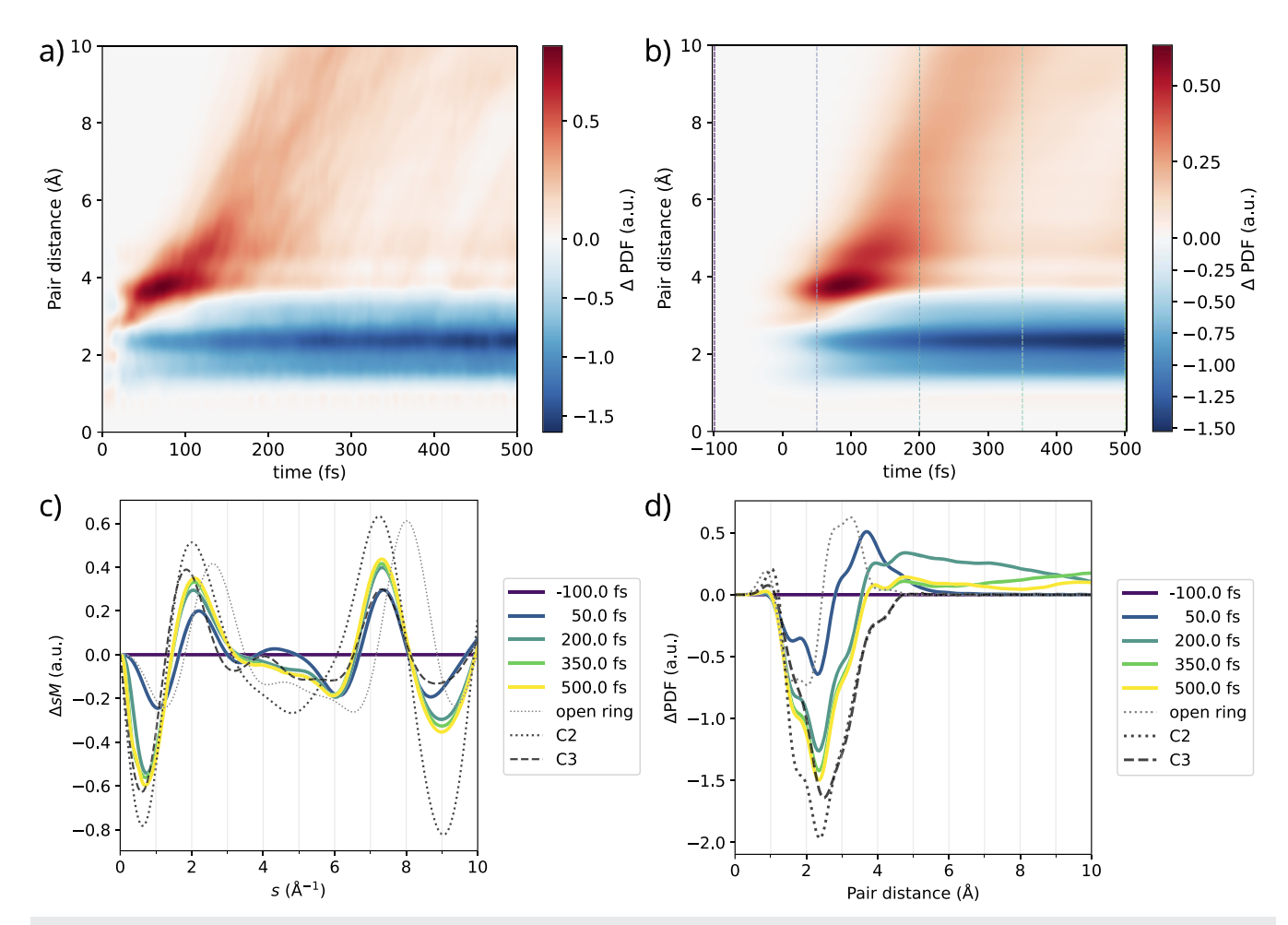


FIG. 4. (a)  $\Delta$ PDF simulated signal. (b) The same signal convoluted with an 80 fs FWHM temporal Gaussian. Color-coded vertical lines correspond to the time slices plotted in panels (c) and (d). (c) Time slices of convoluted modified scattering intensity from -100 to 500 fs. Reference  $\Delta$ sM signals for optimized C2 products, C3 products, and open ring structures are shown in black. (d) Time slices of  $\Delta$ PDF presented in the same manner.

 $5 \text{ Å}^{-1}$ , both signals are negative, but the C2 products contribute a larger negative signal. Differences in the height and location of the first negative and positive peaks (near 0.5 and 2 Å<sup>-1</sup>, respectively) are also observed when comparing the C2 and C3 products.

The presented results account for the first 500 fs of post-excitation dynamics, which could be reliably described using our limited number of trajectories. For longer times, we can expect slow decay of the dissociative signal (above 4 Å in the  $\Delta PDF$ ). Otherwise, the overall shape of the 500 fs time slices should remain relatively unchanged.

#### **B.** Discussion

The primary goal of the present work is to test our ability to predict an experimental measurement *a priori*. However, it is worth discussing what kinds of errors we anticipate might arise from our approach before we have access to the result. Just as it is interesting to see if we can predict the experimental signal, it is also interesting

to see if we can predict which errors might manifest in that prediction. By recording our thinking, this prediction challenge will teach us not only about the accuracy of our methods but also how well we understand them.

Let us first consider the reaction mechanism. A known advantage of *ab initio* molecular dynamics is that it allows us to simulate molecular dynamics with relatively little prior knowledge of the relevant reaction pathway(s) and without enduring a time- and resource-consuming PES fitting procedure. In the present case, we predict that the molecule undergoes ring-opening, followed by dissociation via the C2 and C3 channels. The final photochemical outcomes are not truly predictions because they are known from past photochemical experiments, 94-96 but the initial ring opening step is a prediction and would likely be observable in the experiment. Given that our simulations predict the initial and final states correctly, it seems likely that the prediction of the intermediate ring-opened intermediate state is correct as well. Thus, we expect this prediction to be robust.

Now, we consider the accuracy of our prediction of the experimental observable itself. As mentioned above, GUED is a powerful experiment in part because it can very accurately measure a time-dependent property (interatomic distance) that can also be very accurately predicted by simulation. Given a particular molecular structure, we are confident that the computed experimental observables ( $\Delta$ PDF and its momentum-space counterpart) are accurate. This is not to say that we necessarily predict the correct structures at the correct time.

Although we feel fairly confident about our predictions of mechanisms and observables, our simulations also predict more challenging quantities: branching ratios and timescales. We expect these predictions to be challenging because the calculation of these properties involves the effective exponentiation of relative energies between points on the PES via  $e^{-\Delta E/k_BT}$  ( $\Delta E$  denotes the relative energy,  $k_{\rm B}$  denotes the Boltzmann constant, and T denotes the temperature). This exponentiation can amplify small errors in the PES into large errors in the property of interest. Our simulations are based on a relatively low level of electronic structure theory, and some errors in the PES are inevitable. Therefore, predictions of rates and branching ratios are potentially less robust. A notable exception to this statement would be when the process of interest is governed by ballistic, rather than statistical, motion. The timescale of a ballistic process is governed by the gradient of the PES and the masses of the atoms. In such cases, there is no exponential amplification of error, and a robust prediction is more likely. In turn, we will consider potential errors in our predictions of the C3/C2 branching ratio, the timescale for  $S_2 \rightarrow S_1$  relaxation, and the timescale for subsequent  $S_1 \rightarrow S_0$  relaxation.

Both experiments and past theory suggest that the C3/C2 product ratio has a strong and complicated dependence on pump wavelength. <sup>94–96</sup> This behavior can be attributed to the nonequilibrium vibrational energy distribution driving the dynamics in a short time. <sup>84,86</sup> Our simulations do not take the pump wavelength into account, except rather coarsely by the selection of our initial electronic state. Thus, we anticipate that the error in our predicted branching ratio is a likely source of error in the predicted spectrum.

Next, we will consider the  $S_2 \rightarrow S_1$  relaxation process. To this end, we can estimate the excited state lifetime from existing spectroscopic data.<sup>88,89</sup> Heller describes the relationship between the decay times of the wavepacket's autocorrelation function and the width of absorption spectrum peaks.<sup>97</sup> Since there is a clear vibronic resolution of the first Rydberg state, we can infer a lower bound on the state's half-life in this way. The full width at half maximum (FWHM) of a single subpeak can be estimated to be around 0.02 eV. We can infer the state's half-life by taking the reciprocal of FWHM, yielding 34 fs. Although the decay of S<sub>2</sub> is non-exponential in our simulations, the simulated dynamics are consistent with the inferred experimental timescale; the S<sub>2</sub> population decays to 0.5 in the first 12 fs and then to 0.25 by ~50 fs. Given that this relaxation occurs in the first 1-3 vibrational periods, it appears to be a ballistic, barrierless process; thus, it is not surprising that our prediction here appears robust. However, a previous TRPES experiment by Kuhlman et al. suggests the possibility of a longer sub-ps lifetime in the range of

Finally, we consider the  $S_1 \rightarrow S_0$  relaxation process. In the case of cyclobutanone, the height of the  $S_1$  transition state and the avail-

able vibrational energy will determine the overall kinetics of the process. To estimate possible errors in our  $S_1$  decay rate, we assume the rate-limiting step is traversing the  $S_1$  transition state and apply Rice–Ramsperger–Kassel–Marcus (RRKM) theory to predict the lifetime using a more accurate PES as a function of excess pump energy. This can be thought of as a sanity test on our results; if RRKM on a more accurate surface predicts a much slower (multi-ps) lifetime, this would be a strong indication that our dynamic simulations are much too fast. RRKM assumes the internal energy is randomly distributed among the vibrational modes of the molecule, and the reaction occurs when enough energy accumulates in the reactive mode. The rate constant is evaluated using the following formula:

$$k(E) = \frac{\sigma W^{\ddagger}(E - E_0)}{h\rho(E)},\tag{11}$$

where  $W^{\ddagger}$  denotes the number of accessible vibrational states of the transition state (S<sub>1</sub>TS), excluding those leading to the reaction, and  $\rho$  the density of states of the reactant (S<sub>1</sub>min). The available internal energy of the system is E, and  $E_0$  is the barrier height, both relative to the S<sub>1</sub> minimum in our case. Planck's constant is h, and  $\sigma$  represents the degeneracy of the reaction pathway. We set  $\sigma$  to 2 since there are two symmetry-equivalent ring-opening reactions. Here, we use previously optimized structures from Ref. 85, recalculating the energies and frequencies with the highly accurate complete active space second-order perturbation theory (CASPT2) method. We choose an active space of 10 electrons in 8 orbitals [CASPT2(10,8)] and the 6-31G\* basis. Zero-point energy is included. To calculate the number of states, we use the Beyer–Swinehart algorithm.

To calibrate our surface, we first estimate the half-life upon excitation at 281 nm (4.41 eV) and 255 nm (4.85 eV), which correspond to transient absorption measurements by Kao *et al.*<sup>101</sup> The computed half-lives (1560 and 530 fs at 281 and 255 nm, respectively) are within a factor of four of the shortest experimental timescale (450 fs, which was determined in a global fit including both experiments at 281 and 255 nm<sup>101</sup>). Given that one would expect a fairly strong wavelength dependence for this rate that is not discerned by the global experimental fit, it is difficult to say anything more specific than that RRKM/CASPT2 provides a reasonable estimate of the lifetime.

Now we consider the current simulations. We assume that all excess energy in the 200 nm (6.2 eV) pump pulse is thermalized on S<sub>1</sub> prior to the reaction. Within these assumptions, RRKM predicts an S1 state half-life of 150 fs, which is longer than our simulated timescale by a factor of 2. One can attribute this discrepancy to two different factors: FOMO-CASCI may predict a barrier on S<sub>1</sub> that is too small, and/or the assumption of thermalization on S<sub>1</sub> in RRKM may be invalid here. The entire error is attributable to the assumption of thermalization, we would anticipate very little error in our predicted lifetime. However, if the error is attributed to the FOMO-CASCI barrier height, it is imaginable that we underestimate the timescale for the  $S_1 \rightarrow S_0$  relaxation by a factor of 2, or even more. Keeping in mind that the timescales are exponentially sensitive to errors in the PES, this degree of uncertainty is not surprising. Ultimately, these RRKM/CASPT2 results confirm the sanity of our prediction of a sub-ps lifetime. With additional time and computational effort, simulations based on CASPT2 or another highly

accurate *ab initio* method would allow a more definitive prediction of the timescale.

#### IV. CONCLUSIONS

In this article, we report a prediction of the GUED spectrum of cyclobutanone, excited to the 3s Rydberg state, for comparison to an upcoming experiment. To this end, we applied an *ab initio* molecular dynamics approach based on the TAB nonadiabatic mixed quantum–classical method to simulate the dynamics following the initial pump pulse, and then, we directly simulated the experimental observable. Our simulations show two distinct dissociation pathways that share a common ring-opened intermediate. Analysis of the predicted GUED signal provides guidance on how the ring-opened intermediate, C2 products, and C3 products can be discerned in the spectrum.

We also present our own a priori assessment of the most likely sources of error in our prediction. Although the details are specific to our group's prediction, the general conclusions of our analysis apply broadly to all prediction attempts. The two most likely modes of failure for this prediction challenge are (a) an incorrect prediction of the branching ratio between the C2 and C3 channels and (b) an incorrect prediction of the lifetime for barrier crossing on S<sub>1</sub>. This is because these two processes are governed by statistical motion, and therefore, small errors in relative energies will be amplified via the Boltzmann factor  $e^{-\Delta E/k_BT}$  into large errors in the quantity of interest. In short, we are hopeful that the procedure that we followed in this work is capable of providing a quantitative prediction of the experimental signal, except for those features of the signal that depend exponentially on energy (branching ratios and lifetimes). Of course, significant errors in branching ratios and lifetimes may result in large changes to the signal. Ultimately, these errors arise from the approximate electronic structure methods used in dynamic simulations, more so than the chosen dynamical method.

Importantly, robust predictions of mechanisms and their observable signatures are likely to be sufficient to definitively assign the experimental spectrum, even in the case that predicted lifetimes and branching ratios have significant errors. Thus, even a simulation that fails as a standalone prediction may provide essential insight into the dynamics of cyclobutanone when interpreted in the context of the experimental data.

# SUPPLEMENTARY MATERIAL

The supplementary material for this work includes (1) a document containing optimized molecular structures, a discussion of convergence issues experienced during dynamics, and details of the RRKM calculations and (2) a zip file containing NumPy data files with the predicted spectra.

# **ACKNOWLEDGMENTS**

The authors gratefully acknowledge the support from the National Science Foundation under Grant No. CHE-1954519 and the Institute for Advanced Computational Science (IACS). The

development of the *ab initio* interface to TAB was supported by the U.S. Department of Energy, Office of Science, Office of Basic Energy Sciences, under Award No. DE-SC0021643. J.S. acknowledges a postdoctoral fellowship from IACS.

#### **AUTHOR DECLARATIONS**

# **Conflict of Interest**

The authors have no conflicts to disclose.

#### **Author Contributions**

Jiří Suchan: Investigation (lead); Software (supporting); Writing – original draft (equal); Writing – review & editing (equal). Fangchun Liang: Software (equal). Andrew S. Durden: Software (equal). Benjamin G. Levine: Writing – original draft (equal); Writing – review & editing (equal).

# **DATA AVAILABILITY**

The data that support the findings of this study are available from the corresponding author upon reasonable request.

#### REFERENCES

- <sup>1</sup> A. Zewail, J. Phys. Chem. A **104**, 5660 (2000).
- <sup>2</sup>M. H. M. Janssen, M. Dantus, H. Guo, and A. H. Zewail, Chem. Phys. Lett. 214, 281 (1993).
- <sup>3</sup>B. J. Schwartz and P. J. Rossky, J. Phys. Chem. **98**, 4489 (1994).
- <sup>4</sup>V. S. Batista and D. F. Coker, J. Chem. Phys. **106**, 6923 (1997).
- <sup>5</sup>T. Vreven, F. Bernardi, M. Garavelli, M. Olivucci, M. Robb, and H. Schlegel, J. Am. Chem. Soc. **119**, 12687 (1997).
- <sup>6</sup>M. Ben-Nun and T. J. Martínez, Chem. Phys. Lett. **298**, 57 (1998).
- <sup>7</sup>J. E. Subotnik, A. Jain, B. Landry, A. Petit, W. Ouyang, and N. Bellonzi, Annu. Rev. Phys. Chem. **67**, 387 (2016).
- <sup>8</sup>G. H. Gossel, F. Agostini, and N. T. Maitra, J. Chem. Theory Comput. 14, 4513 (2018).
- <sup>9</sup>R. Crespo-Otero and M. Barbatti, Chem. Rev. 118, 7026 (2018).
- <sup>10</sup>B. F. E. Curchod and T. J. Martínez, Chem. Rev. **118**, 3305 (2018).
- <sup>11</sup>L. Gonzalez and R. Lindh, Quantum Chemistry and Dynamics of Excited States: Methods and Applications (John Wiley & Sons Ltd., Hoboken, NJ, 2021).
- <sup>12</sup>F. Agostini and E. K. U. Gross, Eur. Phys. J. B **94**, 179 (2021).
- <sup>13</sup>L. M. Ibele and B. F. E. Curchod, Phys. Chem. Chem. Phys. 22, 15183 (2020).
- <sup>14</sup>X. Zhang and J. M. Herbert, J. Chem. Phys. **155**, 124111 (2021).
- <sup>15</sup>J. Janos and P. Slavicek, J. Chem. Theory Comput. 19, 8273 (2023).
- <sup>16</sup> A. V. Akimov, J. Comput. Chem. 37, 1626 (2016).
- <sup>17</sup>S. Mai, P. Marquetand, and L. Gonzalez, Wiley Interdiscip. Rev.: Comput. Mol. Sci. **8**, e1370 (2018).
- <sup>18</sup>D. A. Fedorov, S. Seritan, B. S. Fales, T. J. Martinez, and B. G. Levine, J. Chem. Theory Comput. 16, 5485 (2020).
- <sup>19</sup> W. Malone, B. Nebgen, A. White, Y. Zhang, H. Song, J. A. Bjorgaard, A. E. Sifain, B. Rodriguez-Hernandez, V. M. Freixas, S. Fernandez-Alberti, A. E. Roitberg, T. R. Nelson, and S. Tretiak, J. Chem. Theory Comput. 16, 5771 (2020).
- <sup>20</sup>M. Barbatti, M. Bondanza, R. Crespo-Otero, B. Demoulin, P. O. Dral, G. Granucci, F. Kossoski, H. Lischka, B. Mennucci, S. Mukherjee, M. Pederzoli, M. Persico, M. Pinheiro, J. Pittner, F. Plasser, E. S. Gil, and L. Stojanovic, J. Chem. Theory Comput. 18, 6851 (2022).
- <sup>21</sup> M. Barbatti, A. J. A. Aquino, J. J. Szymczak, D. Nachtigallova, P. Hobza, and H. Lischka, Proc. Natl. Acad. Sci. U. S. A. 107, 21453 (2010).

- <sup>22</sup>M. Richter, P. Marquetand, J. Gonzalez-Vazquez, I. Sola, and L. Gonzalez, J. Phys. Chem. Lett. 3, 3090 (2012).
- <sup>23</sup>T. J. Penfold, R. Spesyvtsev, O. M. Kirkby, R. S. Minns, D. S. N. Parker, H. H. Fielding, and G. A. Worth, J. Chem. Phys. 137, 204310 (2012).
- <sup>24</sup>T. Nelson, S. Fernandez-Alberti, A. E. Roitberg, and S. Tretiak, Acc. Chem. Res. 47, 1155 (2014).
- <sup>25</sup>I. Tavernelli, Acc. Chem. Res. **48**, 792 (2015).
- <sup>26</sup>L. Wang, R. Long, and O. V. Prezhdo, Annu. Rev. Phys. Chem. 66, 549 (2015).
- <sup>27</sup>H. H. Fielding and G. A. Worth, Chem. Soc. Rev. **47**, 309 (2018).
- <sup>28</sup>M. S. Schuurman and A. Stolow, Annu. Rev. Phys. Chem. **69**, 427 (2018).
- <sup>29</sup> W. Popp, D. Brey, R. Binder, and I. Burghardt, Annu. Rev. Phys. Chem. 72, 591 (2021).
- <sup>30</sup>F. Talotta, D. Lauvergnat, and F. Agostini, J. Chem. Phys. **156**, 184104 (2022).
- <sup>31</sup>I. D. Dergachev, V. D. Dergachev, M. Rooein, A. Mirzanejad, and S. A. Varganov, Acc. Chem. Res. 56, 856 (2023).
- <sup>32</sup> H. R. Hudock, B. G. Levine, A. L. Thompson, H. Satzger, D. Townsend, N. Gador, S. Ullrich, A. Stolow, and T. J. Martínez, J. Phys. Chem. A 111, 8500 (2007).
- <sup>33</sup>R. Mitric, J. Petersen, M. Wohlgemuth, U. Werner, V. Bonacic-Koutecky, L. Wöste, and J. Jortner, J. Phys. Chem. A 115, 3755 (2011).
- <sup>34</sup>U. De Giovannini, G. Brunetto, A. Castro, J. Walkenhorst, and A. Rubio, ChemPhysChem 14, 1363 (2013).
- <sup>35</sup> A. S. Petit and J. E. Subotnik, J. Chem. Phys. **141**, 154108 (2014).
- <sup>36</sup>S. A. Fischer, C. J. Cramer, and N. Govind, J. Chem. Theory Comput. 11, 4294 (2015).
- <sup>37</sup> T. S. Nguyen, J. H. Koh, S. Lefelhocz, and J. Parkhill, J. Phys. Chem. Lett. 7, 1590 (2016).
- <sup>38</sup> R. Dsouza, X. Cheng, Z. Li, R. J. D. Miller, and M. A. Kochman, J. Phys. Chem. A 122, 9688 (2018).
- <sup>39</sup>F. P. Bonafé, F. J. Hernández, B. Aradi, T. Frauenheim, and C. G. Sánchez, J. Phys. Chem. Lett. 9, 4355 (2018).
- <sup>40</sup> M. F. Gelin, X. Huang, W. Xie, L. Chen, N. Došlić, and W. Domcke, J. Chem. Theory Comput. 17, 2394 (2021).
- <sup>41</sup> M. A. Kochman, B. Durbeej, and A. Kubas, J. Phys. Chem. A **125**, 8635 (2021).
- <sup>42</sup>R. Borrego-Varillas, A. Nenov, P. Kabaciński, I. Conti, L. Ganzer, A. Oriana, V. K. Jaiswal, I. Delfino, O. Weingart, C. Manzoni, I. Rivalta, M. Garavelli, and G. Cerullo, Nat. Commun. 12, 7285 (2021).
- <sup>43</sup>C. Xu, K. Lin, D. Hu, F. L. Gu, M. F. Gelin, and Z. Lan, J. Phys. Chem. Lett. 13, 661 (2022).
- <sup>44</sup> P. Chakraborty, Y. Liu, S. McClung, T. Weinacht, and S. Matsika, J. Phys. Chem. A 126, 6021 (2022).
- <sup>45</sup> M. C. Silfies, A. Mehmood, G. Kowzan, E. G. Hohenstein, B. G. Levine, and T. K. Allison, J. Chem. Phys. **159**, 104304 (2023).
- <sup>46</sup>L. Young, K. Ueda, M. Gühr, P. H. Bucksbaum, M. Simon, S. Mukamel, N. Rohringer, K. C. Prince, C. Masciovecchio, M. Meyer *et al.*, J. Phys. B: At., Mol. Opt. Phys. 51, 032003 (2018).
- <sup>47</sup>M. Nisoli, P. Decleva, F. Calegari, A. Palacios, and F. Martín, Chem. Rev. 117, 10760 (2017).
- <sup>48</sup>M. Kowalewski, B. P. Fingerhut, K. E. Dorfman, K. Bennett, and S. Mukamel, Chem. Rev. **117**, 12165 (2017).
- <sup>49</sup>S. P. Neville, M. Chergui, A. Stolow, and M. S. Schuurman, Phys. Rev. Lett. **120**, 243001 (2018).
- <sup>50</sup> X. Li, N. Govind, C. Isborn, A. E. I. DePrince, and K. Lopata, Chem. Rev. 120, 9951 (2020).
- <sup>51</sup> K. S. Zinchenko, F. Ardana-Lamas, I. Seidu, S. P. Neville, J. van der Veen, V. U. Lanfaloni, M. S. Schuurman, and H. J. Worner, Science 371, 489 (2021).
- <sup>52</sup>C. Cheng, V. Singh, S. Matsika, and T. Weinacht, J. Phys. Chem. A **126**, 7399 (2022)
- <sup>53</sup>V. M. Freixas, D. Keefer, S. Tretiak, S. Fernandez-Alberti, and S. Mukamel, Chem. Sci. 13, 6373 (2022).
- <sup>54</sup>M. Centurion, T. J. Wolf, and J. Yang, Annu. Rev. Phys. Chem. 73, 21 (2022).
- <sup>55</sup>J. Williamson, J. Cao, H. Ihee, H. Frey, and A. Zewail, Nature **386**, 159 (1997).
- <sup>56</sup> H. Ihee, V. Lobastov, U. Gomez, B. Goodson, R. Srinivasan, C. Ruan, and A. Zewail, Science 291, 458 (2001).

- <sup>57</sup>J. Yang, M. Guehr, T. Vecchione, M. S. Robinson, R. Li, N. Hartmann, X. Shen, R. Coffee, J. Corbett, A. Fry, K. Gaffney, T. Gorkhover, C. Hast, K. Jobe, I. Makasyuk, A. Reid, J. Robinson, S. Vetter, F. Wang, S. Weathersby, C. Yoneda, M. Centurion, and X. Wang, Nat. Commun. 7, 11232 (2016).
- <sup>58</sup> J. Yang, M. Guehr, X. Shen, R. Li, T. Vecchione, R. Coffee, J. Corbett, A. Fry, N. Hartmann, C. Hast, K. Hegazy, K. Jobe, I. Makasyuk, J. Robinson, M. S. Robinson, S. Vetter, S. Weathersby, C. Yoneda, X. Wang, and M. Centurion, Phys. Rev. Lett. 117, 153002 (2016).
- <sup>59</sup> J. Yang, X. Zhu, T. J. A. Wolf, Z. Li, J. P. F. Nunes, R. Coffee, J. P. Cryan, M. Gühr, K. Hegazy, T. F. Heinz, K. Jobe, R. Li, X. Shen, T. Veccione, S. Weathersby, K. J. Wilkin, C. Yoneda, Q. Zheng, T. J. Martinez, M. Centurion, and X. Wang, Science 361, 64 (2018).
- <sup>60</sup> T. J. A. Wolf, D. M. Sanchez, J. Yang, R. M. Parrish, J. P. F. Nunes, M. Centurion, R. Coffee, J. P. Cryan, M. Gühr, K. Hegazy, A. Kirrander, R. K. Li, J. Ruddock, X. Shen, T. Vecchione, S. P. Weathersby, P. M. Weber, K. Wilkin, H. Yong, Q. Zheng, X. J. Wang, M. P. Minitti, and T. J. Martinez, Nat. Chem. 11, 504 (2019).
- <sup>61</sup> M. Stefanou, K. Saita, D. V. Shalashilin, and A. Kirrander, Chem. Phys. Lett. 683, 300 (2017); Ahmed Zewail (1946-2016) Commemoration Issue of Chemical Physics Letters.
- <sup>62</sup>R. M. Parrish and T. J. Martínez, J. Chem. Theory Comput. 15, 1523 (2019).
- <sup>63</sup> E. G. Champenois, D. M. Sanchez, J. Yang, J. P. F. Nunes, A. Attar, M. Centurion, R. Forbes, M. Gühr, K. Hegazy, F. Ji, S. K. Saha, Y. Liu, M.-F. Lin, D. Luo, B. Moore, X. Shen, M. R. Ware, X. J. Wang, T. J. Martínez, and T. J. A. Wolf, Science 374, 178 (2021).
- <sup>64</sup>Y. Liu, D. M. Sanchez, M. R. Ware, E. G. Champenois, J. Yang, J. P. F. Nunes, A. Attar, M. Centurion, J. P. Cryan, R. Forbes et al., Nat. Commun. 14, 2795 (2023).
- <sup>65</sup>S. P. Weathersby, G. Brown, M. Centurion, T. F. Chase, R. Coffee, J. Corbett, J. P. Eichner, J. C. Frisch, A. R. Fry, M. Gühr, N. Hartmann, C. Hast, R. Hettel, R. K. Jobe, E. N. Jongewaard, J. R. Lewandowski, R. K. Li, A. M. Lindenberg, I. Makasyuk, J. E. May, D. McCormick, M. N. Nguyen, A. H. Reid, X. Shen, K. Sokolowski-Tinten, T. Vecchione, S. L. Vetter, J. Wu, J. Yang, H. A. Dürr, and X. J. Wang, Rev. Sci. Instrum. 86, 073702 (2015).
- <sup>66</sup>This work was first submitted to arXiv on January 15, (2024). https://doi.org/10.48550/arXiv.2401.08069
- <sup>67</sup>M. P. Esch and B. G. Levine, J. Chem. Phys. **152**, 234105 (2020).
- <sup>68</sup>M. P. Esch and B. Levine, J. Chem. Phys. **155**, 214101 (2021).
- <sup>69</sup> A. S. Durden, F. Liang, J. Suchan, A. Teplukhin, and B. G. Levine (2024). "TAB-DMS,," Zenodo. https://doi.org/10.5281/zenodo.10498050
- <sup>70</sup> J. C. Tully, J. Chem. Phys. **93**, 1061 (1990).
- <sup>71</sup> E. R. Bittner and P. J. Rossky, J. Chem. Phys. **103**, 8130 (1995).
- <sup>72</sup> B. J. Schwartz, E. R. Bittner, O. V. Prezhdo, and P. J. Rossky, J. Chem. Phys. **104**, 5942 (1996).
- <sup>73</sup> M. P. Esch, Y. Shu, and B. G. Levine, J. Phys. Chem. A **123**, 2661 (2019).
- <sup>74</sup>M. P. Esch and B. G. Levine, J. Chem. Phys. **153**, 114104 (2020).
- <sup>75</sup> W.-T. Peng, B. S. Fales, and B. G. Levine, J. Chem. Theory Comput. **14**, 4129 (2018).
- <sup>76</sup> A. S. Durden and B. G. Levine, J. Chem. Theory Comput. **18**, 795 (2022).
- <sup>77</sup>S. Gray and D. Manolopoulos, J. Chem. Phys. **104**, 7099 (1996).
- <sup>78</sup>S. Seritan, C. Bannwarth, B. S. Fales, E. G. Hohenstein, C. M. Isborn, S. I. L. Kokkila-Schumacher, X. Li, F. Liu, N. Luehr, J. W. Snyder, Jr., C. Song, A. V. Titov, I. S. Ufimtsev, L.-P. Wang, and T. J. Martínez, Wiley Interdiscip. Rev.: Comput. Mol. Sci. 11, e1494 (2021).
- <sup>79</sup>I. S. Ufimtsev and T. J. Martinez, J. Chem. Theory Comput. 4, 222 (2008).
- $^{\bf 80}$  I. S. Ufimtsev and T. J. Martinez, J. Chem. Theory Comput. 5, 1004 (2009).
- <sup>81</sup>I. S. Ufimtsev and T. J. Martinez, J. Chem. Theory Comput. 5, 2619 (2009).
- <sup>82</sup>B. S. Fales and B. G. Levine, J. Chem. Theory Comput. 11, 4708 (2015).
- <sup>83</sup> E. G. Hohenstein, M. E. F. Bouduban, C. Song, N. Luehr, I. S. Ufimtsev, and T. J. Martinez, J. Chem. Phys. **143**, 014111 (2015).
- <sup>84</sup>L. Liu and W.-H. Fang, J. Chem. Phys. **144**, 144317 (2016).
- <sup>85</sup>S.-H. Xia, X.-Y. Liu, Q. Fang, and G. Cui, J. Phys. Chem. A **119**, 3569 (2015).
- <sup>86</sup>E. W.-G. Diau, C. Kötting, and A. H. Zewail, ChemPhysChem 2, 294 (2001).
- <sup>87</sup> J. C. Hemminger and E. K. C. Lee, J. Chem. Phys. **56**, 5284 (1972).
- 88 A. Udvarhazi and M. A. El-Sayed, J. Chem. Phys. 42, 3335 (1965).
- <sup>89</sup> J. Hemminger, H. A. Carless, and E. K. Lee, J. Am. Chem. Soc. 95, 682 (1973).

- <sup>90</sup> B. G. Levine, A. S. Durden, M. P. Esch, F. Liang, and Y. Shu, J. Chem. Phys. **154**, 090902 (2021)
- <sup>91</sup> P. Slavíček and T. J. Martínez, J. Chem. Phys. **132**, 234102 (2010).
- <sup>92</sup>G. Granucci, M. Persico, and A. Toniolo, J. Chem. Phys. 114, 10608 (2001).
- <sup>93</sup>F. Salvat, A. Jablonski, and C. J. Powell, Comput. Phys. Commun. **165**, 157 (2005)
- 94H. Denschlag and E. K. Lee, J. Am. Chem. Soc. 90, 3628 (1968).

- 95 N. E. Lee and E. K. C. Lee, J. Chem. Phys. 50, 2094 (1969).
- <sup>96</sup>E. K. C. Lee, Acc. Chem. Res. **10**, 319 (1977).
- <sup>97</sup>E. J. Heller, Acc. Chem. Res. **14**, 368 (1981).
- $^{\bf 98}$  T. S. Kuhlman, T. I. Solling, and K. B. Moller, ChemPhysChem  $\bf 13,820$  (2012).
- <sup>99</sup>R. A. Marcus, J. Chem. Phys. **20**, 359 (1952).
- <sup>100</sup>T. Beyer and D. F. Swinehart, Commun. ACM **16**, 379 (1973).
- 101 M.-H. Kao, R. K. Venkatraman, M. N. R. Ashfold, and A. J. Orr-Ewing, Chem. Sci. 11, 1991 (2020).